Quantum transport observed in films of the magnetic topological semimetal EuSb$_2$

Mizuki Ohno,[1,2] Masaki Uchida [1,2,3,4,*] Ryosuke Kurihara,[5,6] Susumu Minami [7] Yusuke Nakazawa,[1,2] Shin Sato,[1,2]
Markus Kriener [6] Motoaki Hirayama,[1,6] Atsushi Miyake,[5] Yasujiro Taguchi,[6] Ryotaro Arita [1,6]
Masashi Tokunaga [5,6] and Masashi Kawasaki[1,2,6]

[1]*Department of Applied Physics, University of Tokyo, Tokyo 113-8656, Japan*
[2]*Quantum-Phase Electronics Center (QPEC), University of Tokyo, Tokyo 113-8656, Japan*
[3]*PRESTO, Japan Science and Technology Agency (JST), Tokyo 102-0076, Japan*
[4]*Department of Physics, Tokyo Institute of Technology, Tokyo 152-8550, Japan*
[5]*The Institute for Solid State Physics (ISSP), The University of Tokyo, Kashiwa, Chiba 277-8581, Japan*
[6]*RIKEN Center for Emergent Matter Science (CEMS), Wako 351-0198, Japan*
[7]*Department of Physics, University of Tokyo, Tokyo 113-8656, Japan*

We report fabrication of EuSb$_2$ single-crystalline films and investigation of their quantum transport. First-principles calculations demonstrate that EuSb$_2$ is a magnetic topological nodal-line semimetal protected by nonsymmorphic symmetry. Observed Shubnikov-de Haas oscillations with multiple frequency components exhibit small effective masses and two-dimensional field-angle dependence even in a 250 nm thick film, further suggesting possible contributions of surface states. This finding of the high-mobility magnetic topological semimetal will trigger further investigation of exotic quantum transport phenomena by controlling magnetic order in topological semimetal films.

I. INTRODUCTION

Topological semimetals are characterized by nontrivial band crossings at nodal points or nodal lines in the momentum space [1–5]. In topological nodal-point semimetals, Dirac or Weyl semimetals, these gapless points give rise to exotic quantum transport phenomena [3,4]. Under magnetic fields, for example, Fermi arcs of the surface state merge with the bulk state and form so-called Weyl orbits [6,7], as recently observed in its quantum Hall state [8–11].

Topological nodal line semimetals (TNLSMs) are characterized by the Zak phase [12] in loops encircling the nodal lines. It has been theoretically suggested that this topological feature appears in bulk [13,14] and surface [15–19] quantum oscillations. In this context, it is important to prepare high-mobility films of TNLSMs. On the other hand, many compounds which possess nodal lines without spin-orbit coupling (SOC) turn into topological insulators or nodal point semimetals when considering SOC [20,21]. In order to protect these nodal lines from gapping by strong SOC, nonsymmorphic symmetry is required [20–22].

In general, time-reversal symmetry breaking destroys the robustness of nodal lines [23], while they remain stable only when the magnetic ordering still respects space group symmetries [24,25]. Therefore, there are very few reports about intrinsic magnetic TNLSMs under SOC (single-layer GdAg$_2$ [26,27] and GdSbTe [28,29]). Many of the nodes are slightly

gapped on the entire lines (Fe$_3$GeTe$_2$ [30,31] and Fe$_3$X (X = Ga, Al) [32]) or except the Weyl points (Co$_3$Sn$_2$S$_2$ [33] and Co$_2$MnGa [34–36]) under SOC. Moreover, quantum oscillations have not been observed in all of these compounds. Hence, to identify new magnetic TNLSMs strongly calls for exploring unique quantum transport phenomena.

CaSb$_2$ is a novel TNLSM where nodal lines are protected by twofold screw symmetry along the b axis even in the presence of SOC [37]. Recently, superconductivity has also been observed in polycrystalline samples [38]. In EuSb$_2$, on the other hand, large magnetic moments are expected to be introduced while keeping the unique crystal structure. Although antiferromagnetic (AFM) ordering of nearly Eu^{2+} spins has been investigated in the 1980s [39,40], electronic structures and transport properties have long been unknown for EuSb$_2$. Here we demonstrate that EuSb$_2$ is an magnetic TNLSM protected by nonsymmorphic symmetry of the space group $P2_1/m$. We fabricate single-crystalline EuSb$_2$ films by molecular beam epitaxy and investigate their magnetotransport. Observed Shubnikov-de Haas (SdH) oscillations with multiple frequency components indicate small effective masses and two-dimensional (2D) field-angle dependence characteristics in topological semimetals.

II. EXPERIMENTAL METHODS

EuSb$_2$ epitaxial films were grown on single-crystalline $(11\bar{2}0)$ Al$_2$O$_3$ substrates in an Epiquest RC1100 chamber. The molecular beams were simultaneously provided from conventional Knudsen cells containing 3N Eu and 6N Sb. The growth temperature was set at 850 °C, and the beam

*Author to whom correspondence should be addressed: m.uchida@phys.titech.ac.jp

equivalent pressures, measured by an ionization gauge, were set to 1×10^{-5} Pa for Eu and 4.0×10^{-4} Pa for Sb, considering the Eu-Sb binary phase diagram [41]. The film thicknesses were typically set at 250 nm for structural characterization and magnetotransport measurements, and 750 nm for magnetization measurements. The growth rate was about 0.3 Å/s.

High-field resistivity and magnetization measurements were performed at the International MegaGauss Science Laboratory in the Institute for Solid State Physics at the University of Tokyo. Resistivity up to 58 T was measured by a standard four-probe method for 200 μm-width multiterminal Hall bars, using a nondestructive pulsed magnet [42]. Temperature dependence was also measured using a Quantum Design physical properties measurement system. Magnetization up to 27 T was measured by a conventional induction method with coaxial pickup coil [43]. Temperature dependence was also measured using a superconducting quantum interference device magnetometer in a Quantum Design magnetic property measurement system.

First-principles calculations of the band structure with SOC were performed by using the VASP package [44–46], with the experimentally determined lattice constants [39]. The generalized gradient approximation of Perdew-Burke-Ernzerhof was adopted for the exchange-correlation functional [47]. $16 \times 16 \times 10$ k-point mesh with Monkhorst-Pack scheme [48] was used for the Brillouin zone sampling of the primitive cell and Gaussian smearing with a width of 0.02 eV was applied.

III. RESULTS AND DISCUSSION

Figure 1(a) shows the crystal structure of EuSb$_2$. This structure is characterized by Sb zigzag chains running parallel to the b axis and mirror planes in the ac plane. This Sb chain forms Sb$_n^{n-}$ and the valence of Eu becomes divalent (Eu^{2+}). These Eu spin moments are oriented along the [010] direction and antiferromagnetically ordered with a propagation vector of $(1/2, 0, 0)$, corresponding to the magnetic space group P_a2_1/m [40]. Therefore, this AFM ordering does not break the twofold screw symmetry $(2_1/m)$ which protects the nodal lines on the $k_y = \pi/b$ plane. It is thus expected that the nodal lines stably exist in the AFM phase.

The Brillouin zone and band structure calculated for the AFM phase are presented in Figs. 1(b) and 1(c). While flat bands located between -0.3 and -0.7 eV are attributed to the Eu $4f$ orbitals, dispersive bands crossing E_F originate from the Sb $5p$ ones, resembling TNLSM CaSb$_2$. There are band crossing points at the high-symmetry points Z, A, E, and D as in CaSb$_2$ [37], and which are connected by nodal lines on the $k_y = \pi/b$ plane, as shown in Fig. 1(d). This indicates that EuSb$_2$ is a magnetic TNLSM even in the presence of SOC.

X-ray diffraction (XRD) θ-2θ scan in Fig. 2(a) reveals sharp reflections from the (001) EuSb$_2$ lattice plane without any impurity phases. Figures 2(b) and 2(c) show the epitaxial relation viewed along the out-of-plane c^* axis, with a mismatch of 0.7% between the c axis of the ($11\bar{2}0$) Al$_2$O$_3$ plane and the b axis of the (001) EuSb$_2$ plane. The c axis of EuSb$_2$ is tilted by approximately 13 deg. from the c^* axis perpendicular to the a-b plane. Figure 2(d) shows a cross-section image of the EuSb$_2$ film, taken by high-angle annular dark-field
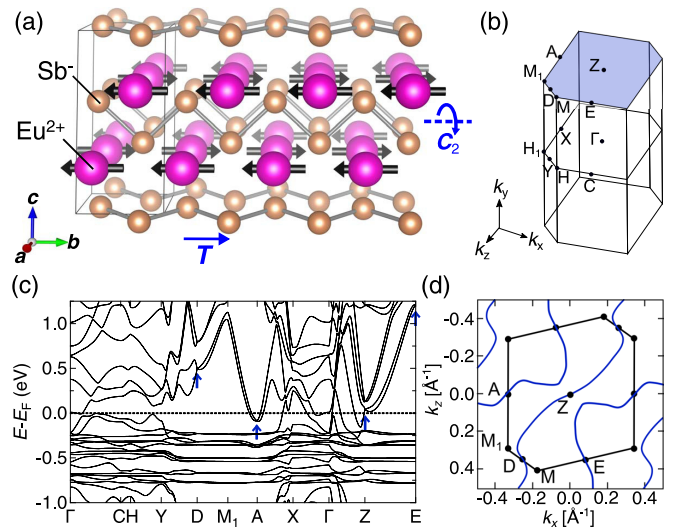
FIG. 1. (a) Crystal structure of EuSb$_2$ with AFM ordering of Eu^{2+} spins at zero field. The solid lines indicate the unit cell, which is doubled along the a axis by the AFM ordering. The screw symmetry that protects the nodal lines is represented in combination with rotational (C_2) and translational (T) operations. (b) Brillouin zone of EuSb$_2$. The Γ-Z line is parallel to the k_y axis. (c) Band structure of EuSb$_2$ calculated for the AFM phase including SOC. Band crossings at the high-symmetry points, which are protected by the twofold screw symmetry, are denoted by blue arrows. (d) Line nodes appearing on the $k_y = \pi/b$ plane in the presence of SOC.

scanning transmission electron microscopy. The periodic arrangement of EuSb$_2$ is clearly confirmed which corresponds to the EuSb$_2$ crystal structure determined by single-crystal XRD [39]. Elemental maps are taken by energy dispersive x-ray spectrometry as shown in Figs. 2(e) and 2(f). The Sb zigzag chains along the b axis are atomically resolved. Further XRD characterization was also performed to confirm high crystallinity and in-plane orientation (see Supplemental Material [50]).

Figure 3(a) summarizes temperature dependence of the resistivity. The resistivity exhibits metallic behavior down to 2 K with a residual resistivity ratio [RRR = $\rho_{xx}(300\,\text{K})/\rho_{xx}(2\,\text{K})$] of 26, reflecting high quality of the film. A clear kink observed at 26.2 K corresponds to the Néel temperature (T_N) [39], which is also seen in temperature dependence of the magnetization (inset). The resistivity decreases rapidly with decreasing temperature below T_N probably due to suppression of the magnetic fluctuations. Figure 3(b) presents out-of-plane magnetic field sweeps of the resistivity up to 58 T at various temperatures. The resistivity at the base temperature of 1.4 K exhibits a cusplike behavior at 14.1 T, which is more clearly seen in its second derivative (inset). This saturation field shifts to the lower values with increasing temperature and then disappears above T_N. Figure 3(c) shows magnetization curves measured at various temperatures. The magnetization taken at 1.4 K increases approximately linearly with field and then saturates at about 7 μ_B, indicating transition from the AFM phase at low fields to the forced ferromagnetic (FM) one. This behavior is consistent with previous magnetization measurements [39]. Below T_N, the saturation field shifts to lower values with increasing
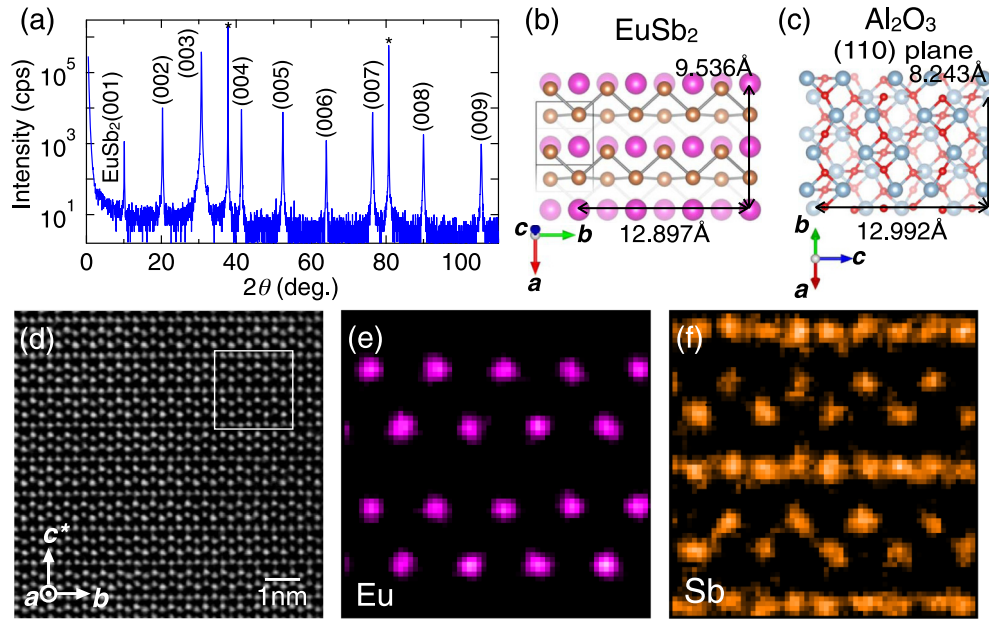
FIG. 2. (a) XRD θ-2θ scan of a EuSb$_2$ film grown on Al$_2$O$_3$ (11$\bar{2}$0) substrate. Al$_2$O$_3$ substrate peaks are marked with an asterisk. Epitaxial relation between (b) the EuSb$_2$ film and (c) the Al$_2$O$_3$ substrate viewed along the out-of-plane direction. (d) Cross-sectional image of the EuSb$_2$ film, taken by high-angle annular dark-field scanning transmission electron microscopy. Energy dispersive x-ray spectrometry map for Eu L (e) and Sb L (f) edges in the boxed region in (d). The Sb zigzag chains along the b axis are atomically resolved.
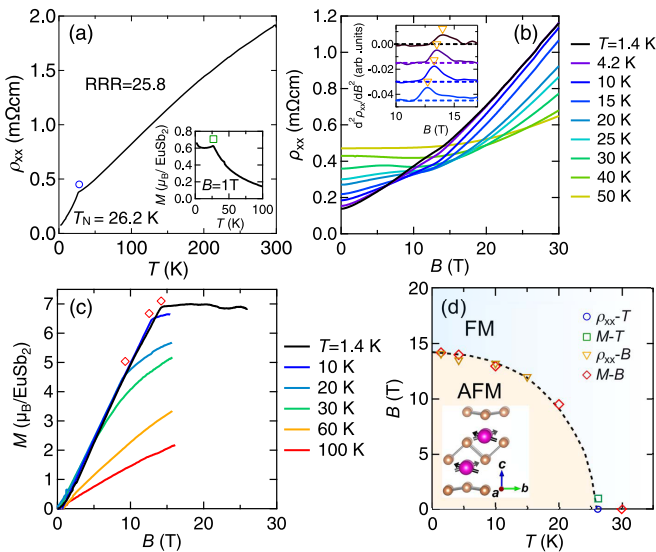
FIG. 3. (a) Temperature dependence of the resistivity ρ_{xx} measured at zero field. The inset shows temperature dependence of the magnetization M, taken with applying an out-of-plane magnetic field of 1.0 T. Both ρ_{xx} and M exhibit a clear kink at the Néel temperature T_N of 26.2 K, as marked by a circle and a square, respectively. (b) ρ_{xx} taken with sweeping the out-of-plane magnetic field at various temperatures. The inset shows the second derivative of ρ_{xx}, where the saturation field is more clearly confirmed as marked by a triangle. (c) Magnetization curve taken at various temperatures, where the saturation field is marked by a diamond. (d) Magnetic phase diagram obtained for out-of-plane magnetic fields ($B \parallel c^*$). The dashed curve represents the boundary between the AFM and FM phases. As shown in the inset, the antiferromagnetically ordered Eu^{2+} spins along the b axis at zero field are gradually canted toward the c^* axis upon increasing the magnetic field.

temperature, as confirmed in the resistivity change. Above T_N, the kink indicating saturation disappears and the magnetization curve follows the Brillouin function. Therefore, the kink indicates the phase transition from AFM to FM phase, where Eu^{2+} $S = 7/2$ spins are polarized along the c^* direction by the magnetic field.

Figure 3(d) summarizes a B-T phase diagram as determined by the above transport and magnetization measurements. Upon increasing the out-of-plane magnetic field, the Eu^{2+} spin moments, which are initially oriented along the b axis at zero field, are gradually canted toward the c^* axis without spin-flop transition. For the in-plane field, on the other band, the magnetization below T_N exhibits a spin-flop transition at 2.4 T, corresponding to reorientation of the spin moments perpendicular to the applied field (see Supplemental Material [50]). EuSb$_2$ exhibits large positive magnetoresistance both in the AFM and FM phases, similar to nonmagnetic TNLSMs (such as ZiSiS [49] and CaSb$_2$ [37]). In the FM phase, the Eu^{2+} localized spins are polarized along the magnetic-field direction and electron scattering by the localized spins is expected to be further suppressed.

The SdH oscillations appear at high fields below 40 K, where the Eu^{2+} spin moments are oriented along the out-of-plane direction and band structures for the FM phase are expected to be realized (see Supplemental Material [50]). Figure 4(a) plots the oscillatory component of the resistivity $\Delta\rho(B)$ as a function of $1/B$ involved at various temperatures. Apparently, there is more than one type of frequency. As shown in Fig. 4(b), the fast Fourier transform (FFT) of $\Delta\rho$ yields three major frequencies at $B_F^\alpha = 247$ T, $B_F^\beta = 372$ T, and $B_F^\gamma = 583$ T and their harmonics. The obtained frequencies suggest the presence of three Fermi pockets (α, β, γ) perpendicular to the c^* axis. As summarized in Table I, the
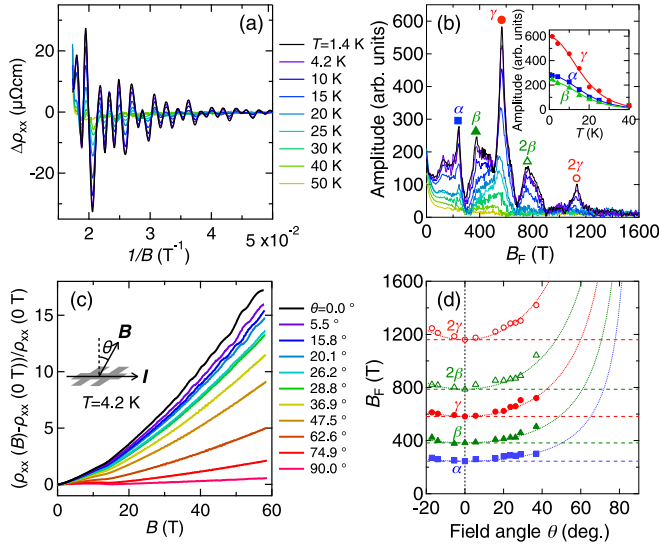
FIG. 4. (a) Temperature dependence of the SdH oscillation $\Delta\rho_{xx}$, plotted against $1/B$ after subtracting a smooth background from ρ_{xx}. (b) FFT spectra of the SdH oscillation $\Delta\rho_{xx}$ for the same set of temperatures. As shown in the inset, temperature dependence of the FFT amplitudes of α, β, and γ peaks is well fitted by the Lifshitz-Kosevich formula. (c) Magnetoresistance $(\rho_{xx}(B) - \rho_{xx}(0\,\mathrm{T}))/\rho_{xx}(0\,\mathrm{T})$ taken with rotating the magnetic field direction at 4.2 K. The field angle θ is measured from the normal direction. (d) Field angle dependence of the oscillation frequencies obtained from the FFT spectra at 4.2 K. All the peaks follow a $\cos\theta^{-1}$ dependence (dotted curves) rather than being constant (dashed curves).

Fermi surface cross-section areas A_F perpendicular to the applied magnetic field are calculated to be 2.3, 3.6, and 5.6 $\times$ 10^{-2} Å^{-2}, using the Lifshitz-Onsager relation, $B_F = \frac{\hbar}{2\pi e}A_F$ with the electron charge e and the reduced Planck constant $\hbar$. These cross-sectional areas are typically small, taking only $\sim$2% of the entire BZ on the k_x-k_y plane.

The FFT amplitudes of these three peaks gradually decrease with elevating temperature. As confirmed in the inset, their temperature dependence can be suitably fitted using the standard Lifshitz-Kosevich formula with thermal damping factors

$$\Delta R(T) \propto \frac{2\pi^2 k_B T/\hbar\omega_c}{\sinh(2\pi^2 k_B T/\hbar\omega_c)}, \tag{1}$$

where k_B is Boltzman constant and $\omega_c = \frac{eB}{m^*}$ the cyclotron frequency. The effective masses m^* are estimated as small as about $0.11m_0$ for all three peaks with the free electron mass m_0, as listed in Table I. Importantly, this value is comparable to or even smaller than one reported in many other topological semimetals, e.g., $0.049m_0$ (bulk) [42] and $0.27m_0$ (surface)

TABLE I. Parameters for the three Fermi pockets extracted from the SdH oscillations.

Carrier	B_F (T)	A_F (Å^{-2})	m^* (m_0)	v_F (10^5 ms^{-1})
α	247	0.023	0.109	3.66
β	372	0.036	0.113	4.39
γ	566	0.056	0.117	5.24

[11] in Cd$_3$As$_2$, $0.07m_0$ (bulk) [54] and $0.50m_0$ (surface) [55] in TaAs, and 0.04–$0.18m_0$ (bulk) [56] in ZrSiS. The Fermi velocity $v_F = \frac{\hbar}{m^*}\sqrt{\frac{A_F}{\pi}}$ is also estimated as large as $\sim 4 \times 10^5$ ms^{-1}, similar to other topological semimetals [11,42,54–56]. More detailed analysis of the SdH oscillations indicates that the mobility is estimated as high as about 200 cm^2 V^{-1} s^{-1} (for details see Supplemental Material [50]).

Figure 4(c) shows field-angle dependence of the SdH oscillations taken at 4.2 K. The magnetoresistance is significantly suppressed with rotation of the field direction from the out-of-plane ($\theta = 0°$, $B \parallel c^*$) to the in-plane ($\theta = 90°$, $B \parallel a$-b) direction. In addition, peaks and valleys of the oscillations shift to higher fields upon increasing θ. As confirmed in Fig. 4(d), although the oscillation amplitude becomes small and it is difficult to follow the frequency at higher angles ($\theta > 40°$), all frequencies extracted from the FFT spectra can be fitted to $1/\cos\theta$, indicating that the quantum transport observed in these EuSb$_2$ films originates from the 2D electronic structure.

One possible origin of the 2D field-angle dependence is that EuSb$_2$ hosts a 2D bulk Fermi surface structure. However, most of the calculated Fermi surfaces are three-dimensional (3D), except only one 2D-like Fermi surface with low Fermi velocity (for details see Supplemental Materials [50]). Another possible origin is the quantum confinement effect. When the film thickness is comparable to the de Broglie wavelength of the carriers, the 3D bulk state is confined to form a 2D quantum-well state. However, the film thickness of 250 nm is considered large enough to maintain the 3D state, because even in Dirac semimetal Cd$_3$As$_2$ with extremely low carrier density and large Fermi velocity exhibits a 3D state above 100 nm film thickness [42]. A third possibility is surface states of EuSb$_2$. By fitting $\Delta\rho_{xx}$ using the LK formula, we obtain nontrivial Berry phases for the β and γ pockets (for details see Supplemental Material [50]). These bands may be nontrivial surface states, which are likely to be protected by the combination of twofold screw and time reversal symmetry. Another possibility is that they are trivial surface states formed on the (001) polar surface, which can also obtain nontrivial phases with the Rashba splitting. In any case, it is not obvious why the 2D conduction state is much more dominant than the 3D state and further studies are needed to determine its origin.

IV. CONCLUSION

In summary, we have fabricated single-crystalline EuSb$_2$ films by molecular beam epitaxy and have studied quantum transport at high fields. First-principles calculations have demonstrated that EuSb$_2$ hosts topological nodal lines protected by nonsymmorphic symmetry, which remains preserved even under AFM ordering. Effective masses extracted from multiple SdH oscillations are fairly small, which is characteristic of topological semimetals. The 2D field-angle dependence of the SdH oscillations suggests the possibility of surface quantum transport in EuSb$_2$. Our finding of the magnetic TNLSM and observation of quantum transport will stimulate further investigations of exotic quantum transport as represented by Weyl orbit and topological phase transitions in magnetic topological semimetals.

ACKNOWLEDGMENTS

[1] C. Fang, H. Weng, X. Dai, and Z. Fang, Chin. Phys. B **25**, 117106 (2016).

[2] A. A. Burkov, M. D. Hook, and L. Balents, Phys. Rev. B **84**, 235126 (2011).

[3] H.-Z. Lu and S.-Q. Shen, Front. Phys. **12**, 127201 (2017).

[4] S. Wang, B.-C. Lin, A.-Q. Wang, D.-P. Yu, and Z.-M. Liao, Adv. Phys. X **2**, 518 (2017).

[5] N. P. Armitage, E. J. Mele, and A. Vishwanath, Rev. Mod. Phys. **90**, 015001 (2018).

[6] A. C. Potter, I. Kimchi, and A. Vishwanath, Nat. Commun. **5**, 5161 (2014).

[7] C. M. Wang, H. P. Sun, H. Z. Lu, and X. C. Xie, Phys. Rev. Lett. **119**, 136806 (2017).

[8] C. Zhang, A. Narayan, S. Lu, J. Zhang, H. Zhang, Z. Ni, X. Yuan, Y. Liu, J. H. Park, E. Zhang, W. Wang, S. Liu, L. Cheng, L. Pi, Z. Sheng, S. Sanvito, and F. Xiu, Nat. Commun. **8**, 1272 (2017).

[9] B. C. Lin, S. Wang, S. Wiedmann, J. M. Lu, W. Z. Zheng, D. Yu, and Z. M. Liao, Phys. Rev. Lett. **122**, 036602 (2019).

[10] C. Zhang, Y. Zhang, X. Yuan, S. Lu, J. Zhang, A. Narayan, Y. Liu, H. Zhang, Z. Ni, R. Liu, E. S. Choi, A. Suslov, S. Sanvito, L. Pi, H.-Z. Lu, A. C. Potter, and F. Xiu, Nature (London) **565**, 331 (2019).

[11] S. Nishihaya, M. Uchida, Y. Nakazawa, R. Kurihara, K. Akiba, M. Kriener, A. Miyake, Y. Taguchi, M. Tokunaga, and M. Kawasaki, Nat. Commun. **10**, 2564 (2019).

[12] J. Zak, Phys. Rev. Lett. **62**, 2747 (1989).

[13] L. Oroszlány, B. Dóra, J. Cserti, and A. Cortijo, Phys. Rev. B **97**, 205107 (2018).

[14] H. Yang, R. Moessner, and L. K. Lim, Phys. Rev. B **97**, 165118 (2018).

[15] Y. H. Chan, C. K. Chiu, M. Y. Chou, and A. P. Schnyder, Phys. Rev. B **93**, 205132 (2016).

[16] G. Bian, T. R. Chang, H. Zheng, S. Velury, S. Y. Xu, T. Neupert, C. K. Chiu, S. M. Huang, D. S. Sanchez, I. Belopolski, N. Alidoust, P.-J. Chen, G. Chang, A. Bansil, H. T. Jeng, H. Lin, and M. Z. Hasan, Phys. Rev. B **93**, 121113(R) (2016).

[17] A. Yamakage, Y. Yamakawa, Y. Tanaka, and Y. Okamoto, J. Phys. Soc. Jpn. **85**, 013708 (2016).

[18] M. Hirayama, R. Okugawa, T. Miyake, and S. Murakami, Nat. Commun. **8**, 14022 (2017).

[19] M. Hirayama, R. Okugawa, and S. Murakami, J. Phys. Soc. Jpn. **87**, 041002 (2018).

[20] C. Fang, Y. Chen, H. Y. Kee, and L. Fu, Phys. Rev. B **92**, 081201(R) (2015).

[21] S. Kobayashi, Y. Yamakawa, A. Yamakage, T. Inohara, Y. Okamoto, and Y. Tanaka, Phys. Rev. B **95**, 245208 (2017).

[22] Y. X. Zhao and A. P. Schnyder, Phys. Rev. B **94**, 195109 (2016).

[23] R. Okugawa and S. Murakami, Phys. Rev. B **96**, 115201 (2017).

[24] T. Bzdušek, Q. S. Wu, A. Rüegg, M. Sigrist, and A. A. Soluyanov, Nature (London) **538**, 75 (2016).

[25] J. Wang, Phys. Rev. B **96**, 081107(R) (2017).

[26] M. Ormaza, L. Fernández, M. Ilyn, A. Magana, B. Xu, M. J. Verstraete, M. Gastaldo, M. A. Valbuena, P. Gargiani, A. Mugarza, A. Ayuela, L. Vitali, M. Blanco-Rey, F. Schiller, and J. E. Ortega, Nano Lett. **16**, 4230 (2016).

[27] B. Feng, R. W. Zhang, Y. Feng, B. Fu, S. Wu, K. Miyamoto, S. He, L. Chen, K. Wu, K. Shimada, T. Okuda, and Y. Yao, Phys. Rev. Lett. **123**, 116401 (2019).

[28] M. M. Hosen, G. Dhakal, K. Dimitri, P. Maldonado, A. Aperis, F. Kabir, C. Sims, P. Riseborough, P. M. Oppeneer, D. Kaczorowski, T. Durakiewicz, and M. Neupane, Sci. Rep. **8**, 13283 (2018).

[29] R. Sankar, I. P. Muthuselvam, K. R. Babu, G. S. Murugan, K. Rajagopal, R. Kumar, T. C. Wu, C. Y. Wen, W. L. Lee, G. Y. Guo, and F. C. Chou, Inorg. Chem. **58**, 11730 (2019).

[30] B. Chen, J. H. Yang, H. D. Wang, M. Imai, H. Ohta, C. Michioka, K. Yoshimura, and M. H. Fang, J. Phys. Soc. Jpn. **82**, 124711 (2013).

[31] K. Kim, J. Seo, E. Lee, K. T. Ko, B. S. Kim, B. G. Jang, J. M. Ok, J. Lee, Y. J. Jo, W. Kang, J. S. Shim, C. Kim, H. W. Yeom, B. I. Min, B. J. Yang, and J. S. Kim, Nat. Mat. **17**, 794 (2018).

[32] A. Sakai, S. Minami, T. Koretsune, T. Chen, T. Higo, Y. Wang, T. Nomoto, M. Hirayama, S. Miwa, D. Nishio-Hamane, F. Ishii, R. Arita, and S. Nakatsuji, Nature (London) **581**, 53 (2020).

[33] E. Liu, Y. Sun, N. Kumar, L. Muechler, A. Sun, L. Jiao, S. Y. Yang, D. Liu, A. Liang, Q. Xu, Q. Kroder, V. Süß, H. Borrmann, C. Shekhar, Z. Wang, C. Xi, W. Wang, W. Schnelle, S. Writh, Y. Chen, S. T. B. Goennenwein, and C. Felser, Nat. Phys. **14**, 1125 (2018).

[34] G. Chang, S.-Y. Xu, X. Zhou, S.-M. Huang, B. Singh, B. Wang, I. Belopolski, J. Yin, S. Zhang, A. Bansil, Hsin Lin, and M. Zahid Hasan, Phys. Rev. Lett. **119**, 156401 (2017).

[35] A. Sakai, Y. P. Mizuta, A. A. Nugroho, R. Sihombing, T. Koretsune, M. T. Suzuki, N. Takemori, R. Ishii, D. Nishio-Hamane, R. Arita, P. Goswami, and S. Nakatsuji, Nat. Phys. **14**, 1119 (2018).

[36] I. Belopolski, K. Manna, D. S. Sanchez, G. Chang, B. Ernst, J. Yin, S. S. Zhang, T. Cochran, N. Shumiya, H. Zheng, B. Singh, G. Bian, D. Multer, M. Litskevich, X. Zhou, S.-M. Huang, B. Wang, T.-R. Chang, S.-Y. Xu, A. Bansil, C. Felser, H. Lin, and M. Z. Hasan, Science **365**, 1278 (2019).

[37] K. Funada, A. Yamakage, N. Yamashina, and H. Kageyama, J. Phys. Soc. Jpn. **88**, 044711 (2019).

[38] A. Ikeda, M. Kawaguchi, S. Koibuchi, T. Hashimoto, T. Kawakami, S. Yonezawa, M. Sato, and Y. Maeno, Phys. Rev. Materials **4**, 041801(R) (2020).

[39] F. Hulliger and R. Schmelczer, J. Solid State Chem. **26**, 389 (1978).

[40] A. Niggli and F. Hulliger, Z. Kristallogr. **167**, 125 (1984).

[41] M. N. Abdusalyamova and I. G. Vasilyeva, J. Solid State Chem. **184**, 2751 (2011).

[42] M. Uchida, Y. Nakazawa, S. Nishihaya, K. Akiba, M. Kriener, Y. Kozuka, A. Miyake, Y. Taguchi, M. Tokunaga, N.

Nagaosa, Y. Tokura, and M. Kawasaki, Nat. Commun. **8**, 2274 (2017).

[43] H. Yoshida, Y. Okamoto, T. Tayama, T. Sakaktbara, M. Tokunaga, A. Matsuo, Y. Narumi, K. Kindo, M. Yoshida, M. Takigawa, and Z. Hiroi, J. Phys. Soc. Jpn. **78**, 043704 (2009).

[44] G. Kresse and J. Furthmüller, Comput. Mater. Sci. **6**, 15 (1996).

[45] G. Kresse and J. Furthmüller, Phys. Rev. B **54**, 11169 (1996).

[46] G. Kresse and D. Joubert, Phys. Rev. B **59**, 1758 (1999).

[47] J. P. Perdew, M. Ernzerhof, and K. Burke, J. Chem. Phys. **105**, 9982 (1996).

[48] H. J. Monkhorst and J. D. Pack, Phys. Rev. B **13**, 5188 (1976).

[49] R. Sankar, G. Peramaiyan, I. P. Muthuselvam, C. J. Butler, K. Dimitri, M. Neupane, G. N. Rao, M. T. Lin, and F. C. Chou, Sci. Rep. **7**, 40603 (2017).

[50] See Supplemental Material at http://link.aps.org/supplemental/10.1103/PhysRevB.103.165144 for detailed characterization, which includes Refs. [51–53].

[51] K. S. Takahashi, H. Ishizuka, T. I. Murata, Q. Y. Wang, Y. Tokura, N. Nagaosa, and M. Kawasaki, Sci. Adv. **4**, eaar7880 (2018).

[52] G. P. Mikitik and Y. V. Sharlai, Phys. Rev. Lett. **82**, 2147 (1999).

[53] Z. Wang, Y. Zheng, Z. Shen, Y. Lu, H. Fang, F. Sheng, Y. Zhou, X. Yang, Y. Li, C. Feng, and Z.-A. Xu, Phys. Rev. B **93**, 121112(R) (2016).

[54] C. L. Zhang, Z. Yuan, Q. D. Jiang, B. Tong, C. Zhang, X. C. Xie, and S. Jia, Phys. Rev. B **95**, 085202 (2017).

[55] N. L. Nair, M.-E. Boulanger, F. Laliberté, S. Griffin, S. Channa, A. Legros, W. Tabis, C. Proust, J. Neaton, L. Taillefer, and J. G. Analytis, Phys. Rev. B **102**, 075402 (2020).

[56] M. Matusiak, J. R. Cooper, and D. Kaczorowski, Nat. Commun. **8**, 15219 (2017).